

# A Multiscale Investigation of Repolarization Variability and Its Role in Cardiac Arrhythmogenesis

Esther Pueyo,<sup>†‡\$\*</sup> Alberto Corrias,<sup>†</sup> László Virág,<sup>¶</sup> Norbert Jost,<sup>||</sup> Tamás Szél,<sup>¶</sup> András Varró,<sup>¶||</sup> Norbert Szentandrásy,<sup>\*\*</sup> Péter P. Nánási,<sup>\*\*</sup> Kevin Burrage,<sup>†</sup> and Blanca Rodríguez<sup>†</sup>

<sup>†</sup>Department of Computer Science, University of Oxford, Oxford, United Kingdom; <sup>‡</sup>Aragón Institute of Engineering Research, IIS Aragón, Universidad de Zaragoza, Zaragoza, Spain; <sup>\$</sup>Biomedical Research Networking Center in Bioengineering, Biomaterials and Nanomedicine, Zaragoza, Spain; <sup>¶</sup>Department of Pharmacology and Pharmacotherapy, University of Szeged, Szeged, Hungary; <sup>||</sup>Division of Cardiovascular Pharmacology, Hungarian Academy of Sciences, Szeged, Hungary; and <sup>\*\*</sup>Department of Physiology, University of Debrecen, Debrecen, Hungary

**ABSTRACT** Enhanced temporal and spatial variability in cardiac repolarization has been related to increased arrhythmic risk both clinically and experimentally. Causes and modulators of variability in repolarization and their implications in arrhythmogenesis are however not well understood. At the ionic level, the slow component of the delayed rectifier potassium current ( $I_{Ks}$ ) is an important determinant of ventricular repolarization. In this study, a combination of experimental and computational multiscale studies is used to investigate the role of intrinsic and extrinsic noise in  $I_{Ks}$  in modulating temporal and spatial variability in ventricular repolarization in human and guinea pig. Results show that under physiological conditions: i), stochastic fluctuations in  $I_{Ks}$  gating properties (i.e., intrinsic noise) cause significant beat-to-beat variability in action potential duration (APD) in isolated cells, whereas cell-to-cell differences in channel numbers (i.e., extrinsic noise) also contribute to cell-to-cell APD differences; ii), in tissue, electrotonic interactions mask the effect of  $I_{Ks}$  noise, resulting in a significant decrease in APD temporal and spatial variability compared to isolated cells. Pathological conditions resulting in gap junctional uncoupling or a decrease in repolarization reserve uncover the manifestation of  $I_{Ks}$  noise at cellular and tissue level, resulting in enhanced ventricular variability and abnormalities in repolarization such as afterdepolarizations and alternans.

## INTRODUCTION

A large body of research has tried to unravel the mechanisms of lethal arrhythmias. However, the reasons why a particular patient dies on a particular day still remain a mystery. Different hearts can exhibit a very different response to a similar trigger, some developing arrhythmias, whereas others remain in sinus rhythm. Moreover, the same heart and even the same cell can react differently to a similar trigger at different times due to temporal variability and stochastic events. Enhanced temporal and spatial variability in cardiac repolarization has been linked to increased arrhythmic risk in both experimental (1–3) and clinical studies (4,5). The causes of spatiotemporal cardiac repolarization variability are still under investigation but are likely to involve complex multiscale mechanisms from the ionic to the whole organ level.

This study aims at investigating causes and modulators of temporal and spatial variability in ventricular repolarization using a combined experimental and computational approach. On the basis of previous experimental findings (6,7), we hypothesize that fluctuations in ionic currents caused by stochasticity in ion channel behavior contribute to variability in cardiac repolarization, particularly under pathological conditions. We also postulate that electrotonic interactions through intercellular coupling act to mitigate spatiotemporal variability in repolarization dynamics in

tissue, as compared to isolated cells. Our study specifically focuses on investigating the role that stochasticity in the slow component of the delayed rectifier potassium current ( $I_{Ks}$ ) plays in modulating variability in ventricular repolarization in human and guinea pig. Among all ionic currents, the slow kinetics and small channel numbers associated with  $I_{Ks}$  are likely to result in larger stochastic ionic current fluctuations compared to other currents with larger channel numbers and, consequently, reduced fluctuations. Furthermore,  $I_{Ks}$  has been shown to be an important determinant of repolarization stability, especially under reduced repolarization reserve conditions (3,8). Stochasticity in  $I_{Ks}$  has also been shown to determine beating rate irregularity in embryonic chick cells (9).

Our approach to investigate the implications of  $I_{Ks}$  stochasticity in repolarization variability combines experimental and computational investigations in human and guinea pig. Multiscale stochastic models of ventricular electrophysiology are developed, bridging ion channel numbers to whole organ behavior. Intrinsic (random gating) and extrinsic (cell-to-cell differences) noises in  $I_{Ks}$  are included in the models based on experimental data at different scales. Intrinsic noise properties are modeled using a stochastic differential equation (SDE) of Langevin type driven by Wiener noise (10), rather than using discrete Markov processes, for computational efficiency (11). Models are thoroughly validated by comparing simulated and experimental results on ionic current, cellular, tissue, and electrocardiogram (ECG) properties.

Submitted May 2, 2011, and accepted for publication September 27, 2011.

\*Correspondence: [epueyo@unizar.es](mailto:epueyo@unizar.es)

Editor: Andrew McCulloch.

© 2011 by the Biophysical Society  
0006-3495/11/12/2892/11 \$2.00

doi: 10.1016/j.bpj.2011.09.060

There are a number of studies in the literature that have modeled the stochastic behavior of cardiac ion channels using different methodological approaches, e.g., by adding a global fluctuation current (12), by determining the state and lifetimes of channel gates (6), or by using SDEs (13). To the best of our knowledge, four previous studies have included a stochastic  $I_{Ks}$  formulation in ventricular models. Sato et al. (14) introduced a stochastic Langevin equation to describe  $I_{Ks}$  gating dynamics in a rabbit ventricular action potential (AP) model. Their formulation was, however, not based on experimental data, thus limiting the conclusions about fluctuation-induced effects at higher levels. Krogh-Madsen (9) developed a stochastic model of embryonic chick ventricular cells with a mathematical formulation of  $I_{Ks}$  stochastic gating, and Silva et al. (15) combined molecular structural dynamics with electrophysiological modeling to describe  $I_{Ks}$ , but no investigation was conducted in those two studies on the role of  $I_{Ks}$  stochasticity in modulating spatiotemporal variability in repolarization and its link to proarrhythmia, which are major objectives of this study. A very recent work published by Lemay et al. (16) shares these objectives with our study. However, while the paper by Lemay et al., as well as a preliminary work already presented by our group (17), both present a purely computational investigation, this study uses specific experimental data both for the development of the stochastic AP models and for confirmation of simulation predictions. Furthermore, two different species, i.e., guinea pig and human, are investigated in our study, and experimental and computational data are provided to show the validity of the results in the two species. Lemay et al. use a guinea pig model and develop stochastic formulations for different ionic currents based on experimental data from the literature corresponding to a range of different species, including rat, human, or guinea pig.

## MATERIALS AND METHODS

### Stochastic cell and tissue models

$I_{Ks}$  stochastic gating was simulated by introducing intrinsic noise into two mathematical AP models, namely the human ten Tusscher-Panfilov (TP06) (18) and the guinea pig Faber-Rudy (FR07) (19). In both models, the Hodgkin-Huxley formulation for the  $I_{Ks}$  gating variables was replaced by a novel formulation based on the Langevin equation (20). In the case of the TP06 model, the ordinary differential equation defining the gating variable  $x_s$ ,

$$dx_s = \frac{x_{s\infty}(V) - x_s}{\tau_{xs}(V)} dt, \quad (1)$$

was replaced by the following SDE:

$$dx_s = \frac{x_{s\infty}(V) - x_s}{\tau_{xs}(V)} dt + \frac{1}{(\tau_{xs}(V)n_{Ks})^{\frac{1}{2}}} (x_{s\infty}(V) - (1 - 2x_{s\infty}(V))x_s^{\frac{1}{2}}) dW, \quad (2)$$

where  $V$  is the transmembrane voltage,  $x_{s\infty}$  and  $\tau_{xs}$  are the steady-state value of  $x_s$  and the time constant to reach that steady-state value (both being func-

tions of  $V$ ),  $n_{Ks}$  is the number of  $I_{Ks}$  channels in the cell membrane, and  $W$  represents a Wiener process. In the case of the FR07 model, SDEs analogous to Eq. 2 were formulated for the two  $I_{Ks}$  gating variables  $x_{s1}$  and  $x_{s2}$ . As  $n_{Ks}$  becomes large, fluctuations in  $x_s$  introduced by the Wiener increment  $dW$  in Eq. 2 are decreased in magnitude, and the SDE is reduced to the standard ordinary differential equation of the TP06 model shown in Eq. 1 (analogously for the FR07 model).

Extrinsic noise was also included in the investigations by incorporating cell-to-cell differences in the number of  $I_{Ks}$  channels ( $n_{Ks}$ ). Briefly,  $n_{Ks}$  was obtained from a truncated Gaussian distribution with mean  $m_n$  and standard deviation  $\sigma_n$ . The mean  $m_n$  was taken as the estimated  $n_{Ks}$  value derived as described in the Noise analysis subsection, whereas the standard deviation  $\sigma_n$  was computed as one-half of  $m_n$  to match the dispersion values obtained from experimental  $I_{Ks}$  current data, as described in the Supporting Material. The truncation of the Gaussian distribution was defined to set bounds on  $n_{Ks}$  that guaranteed that physiologically plausible AP durations were always obtained in the simulations (see the Supporting Material).

Transmural heterogeneities in the densities of  $I_{Ks}$  and  $I_{to}$  (transient outward potassium current) were introduced as in previous studies (18,21). A monodomain reaction-diffusion equation was used to model the propagation of the cellular APs in a transmural one-dimensional (1D) fiber and a ventricular mesh (22). Pseudo-ECG (extracellular unipolar potential) traces were computed as in (21), and were delineated using a wavelet-based system. Three stimulation protocols (periodic, decelerating frequency change, and dynamic restitution) were applied in single cell and tissue simulations. Further details are provided in the Supporting Material.

## Experimental data

### Experimental $I_{Ks}$ current traces

Ventricular myocytes were enzymatically isolated from undiseased human donor hearts. Nisoldipine (1 mM) was used to block  $I_{CaL}$  (L-type calcium current), and E-4031 (1–5  $\mu$ M) to inhibit  $I_{Kr}$  (rapid delayed rectifier potassium current).  $I_{Ks}$  currents were recorded with Axopatch-1D and Axopatch-200B patch-clamp amplifiers (Axon Instruments, Foster City CA) using the whole-cell configuration of the patch-clamp technique, and were digitized using a 333 kHz analog-to-digital converter (Digidata 1200, Axon Instruments). Low-pass filtering at 1 kHz was applied. Experiments were performed at 37°C.

### Experimental APs in single myocytes

**Dog and human.** Ventricular myocytes were enzymatically isolated from dog and human hearts. Transmembrane potentials were recorded using 3 M KCl-filled sharp glass microelectrodes connected to the input of an Axoclamp-2B amplifier (Axon Instruments). The cells were paced at 1 Hz using 1-ms current pulses with 120% threshold amplitude. For drug experiments, an incubation period of 5–6 min was applied to develop the steady-state drug effect. APs were digitized at 200 kHz using Digidata 1200 A/D card (Axon Instruments).

**Guinea pig.** Ventricular myocytes were enzymatically isolated from guinea pig hearts, corresponding to the left ventricle base and apex subendo and subepicardial regions. The cell membrane potential was measured with the perforated patch method. The cells were paced at 1 Hz using 0.3-ms current pulses with  $18 \pm 2$  nA amplitude. APs were digitized at 10 kHz, with a 5 kHz low-pass Bessel filter.

All experiments were performed at 37°C.

### Experimental APs in tissue

**Dog.** Hearts were immediately removed from anesthetized adult mongrel dogs and rinsed in oxygenated Locke's solution at 37°C. Midmyocardial ventricular preparations were stimulated at 1 Hz using 2-ms voltage pulses twice diastolic threshold in amplitude.

**Human.** Human cardiac tissue was stored in cardioplegic solution at 4°C for 4–8 h, and papillary muscles were obtained from the right ventricle.

Preparations were stimulated at 1 Hz and were continuously superfused with Locke's solution. All experiments were performed at 37°C. Transmembrane potentials were recorded using conventional microelectrode technique.

For drug experiments, an incubation period of 60 min was applied to develop the steady-state drug effect.

### Experiment approval by review boards

The human experimental protocol complied with the Declaration of World Medical Association proclaimed in Helsinki and was approved by the Ethical Review Board of the Albert Szent-Györgyi Medical University (No. 51-57/1997 OEj) and by the Scientific and Research Ethical Committee of the Medical Scientific Board at the Hungarian Ministry of Health (ETT-TUKEB), under ethical approval No. 4991-0/2010-1018EKU (339/PI/10). The guinea pig experiments were carried out in accordance with the UK Home Office guidance on the Operation of Animals (Scientific Procedures) Act of 1986. The dog experiments were carried out in compliance with the Guide for the Care and Use of Laboratory Animals (National Institutes of Health publication No. 85-23, revised 1985), and the protocols were approved by the Department of Animal Health and Food Control of the Ministry of Agriculture and Rural Development, Hungary (15.1/01031/006/2008).

More details about the experimental data and methods used in this study can be found in the [Supporting Material](#).

### Noise analysis

Fluctuation analysis of experimental and simulated macroscopic current measurements was applied to estimate the parameters required to model stochastic  $I_{Ks}$  fluctuations in human and guinea pig. We assumed  $n_{Ks}$  channels to gate independently and the current through each individual channel in any state to be either zero or the unitary current ( $i_{Ks}$ ). Then, the following relationship between the variance  $\sigma_{Ks}^2$  and the mean  $m_{Ks}$  of the macroscopic  $I_{Ks}$  current holds (23):

$$\sigma_{Ks}^2 = m_{Ks} i_{Ks} - (1/n_{Ks})m_{Ks}^2. \quad (3)$$

In this study, a combination of stationary and nonstationary fluctuation methods was applied on experimental and simulated human recordings to identify the number  $n_{Ks}$  of  $I_{Ks}$  channels in the stochastic cell models. In brief, a value for the single channel current,  $i_{Ks}$ , was obtained from the experiments, and that value was taken as a reference to identify the number of  $I_{Ks}$  channels that, used in the stochastic simulations, led to a best match with the experimental  $i_{Ks}$  value. Specifically, experimental  $I_{Ks}$  current traces were measured in human ventricular myocytes after applying 5000-ms depolarizing voltage pulses from -40 mV to test potentials ranging from -10 to 50 mV (24). Because reliable  $I_{Ks}$  measurements could not be obtained immediately after the delivery of each pulse, but only ~100 ms after the transient change elicited by the pulse, ensemble mean and variance of the available  $I_{Ks}$  traces were computed at steady state for each of the test potentials. The nonstationary fluctuation analysis was used to estimate  $n_{Ks}$  and  $i_{Ks}$  by fitting the parabolic function of Eq. 3 to the variance-mean  $I_{Ks}$  data corresponding to the different test potentials (25). The mean channel open probability ( $p_{Ks}$ ) was then computed as

$$p_{Ks} = \frac{m_{Ks}}{(i_{Ks} n_{Ks})}. \quad (4)$$

The mean channel open probability,  $p_{Ks}$ , was estimated at 50 mV (corresponding to the highest open probability). Some studies have reported that this method provides reliable estimates of  $p_{Ks}$ , but not of  $i_{Ks}$  or  $n_{Ks}$ , which cannot be robustly estimated unless some constraints on the variables to be estimated are imposed (26), particularly when voltages associated with low  $p_{Ks}$  are considered. Therefore, once an estimate of  $p_{Ks}$  was obtained at

a specific voltage level (in this study, at 50 mV), a second method based on the stationary fluctuation analysis was used to estimate  $i_{Ks}$  (27). In this case, power spectral densities (PSDs) of mean-subtracted  $I_{Ks}$  current traces were computed, once  $I_{Ks}$  has reached steady state at the specific test potential. The unitary current  $i_{Ks}$  was estimated as the ratio between the integral of the averaged PSD divided by the product of  $1-p_{Ks}$  and the time-averaged mean current (28).

Taking that experimental  $i_{Ks}$  estimate as a reference, fluctuation analysis was applied on simulated  $I_{Ks}$  current traces (obtained using the same voltage clamp protocol as in the experiments) and the best possible number of  $I_{Ks}$  channels in the stochastic human model was determined. In the simulations, reliable  $I_{Ks}$  measurements could be obtained from the beginning of the recordings, thus both the stationary and nonstationary methods could be applied on the simulated  $I_{Ks}$  traces at 50 mV. Results from the two methods were contrasted to ensure consistency of the identified  $n_{Ks}$  value.

For the guinea pig stochastic model, we considered the upper limit for the  $I_{Ks}$  unitary conductance estimated by Walsh et al. in experiments obtained with a filter cut-off frequency of 200 Hz (29). That value has been reported to be approximately half of the value found for human  $I_{Ks}$  currents expressed in *Xenopus* oocytes (28,30). We then used the frequency dependence data provided in (30) to extrapolate the unitary conductance value corresponding to 1 kHz, which is the cut-off frequency used in the human experiments, and we divided it by two to represent guinea pig myocytes. That process provided us with an estimate of 3.3 pS for the  $I_{Ks}$  unitary conductance in guinea pig, which we used to identify the corresponding number  $n_{Ks}$  of  $I_{Ks}$  channels in the model.

## RESULTS AND DISCUSSION

### Microscopic ion channel fluctuations modulate macroscopic ionic current kinetics

Intrinsic noise due to  $I_{Ks}$  stochastic gating was introduced in the model with parameters obtained from experimental traces using the approach described in the [Materials and Methods](#) section. In human, fluctuation analysis applied to experimental  $I_{Ks}$  data is presented in [Fig. 1 A](#)—variance-mean plots of steady  $I_{Ks}$  traces at different test potentials (*top third panel*), averaged  $I_{Ks}$  power spectral density at 50 mV (*top fourth panel*), and estimated single channel current (*bottom right panel*). As shown in [Fig. 1 A](#), the single channel current estimated from experimental recordings of macroscopic  $I_{Ks}$  traces at 50 mV was  $i_{Ks} = 0.762$  pA. This is in good agreement with previous values reported in the literature for currents formed by human KvLQT1 and minK subunits injected into *Xenopus* oocytes, where mean  $i_{Ks}$  was found to be 0.6 pA (28), and 0.8 pA (30). In guinea pig,  $I_{Ks}$  unitary conductance was estimated using available data from the literature (29,30), as described in the [Methods](#) section.

The  $i_{Ks}$ /unitary conductance values obtained from the experiments were then used to identify the number of  $I_{Ks}$  channels to be considered in the stochastic ventricular models, assuming that unitary current/conductance is uniform across cells (31). The number of  $I_{Ks}$  channels identified for the different simulated cell types was: in human,  $n_{Ks} = 12,000$  for endocardial (endo) and epicardial (epi) cells and  $n_{Ks} = 3000$  channels for midmyocardial (mid) cells; in guinea pig,  $n_{Ks} = 20,000$  for epi, 6286 for endo, and 2286 for mid cells. To illustrate the time and frequency

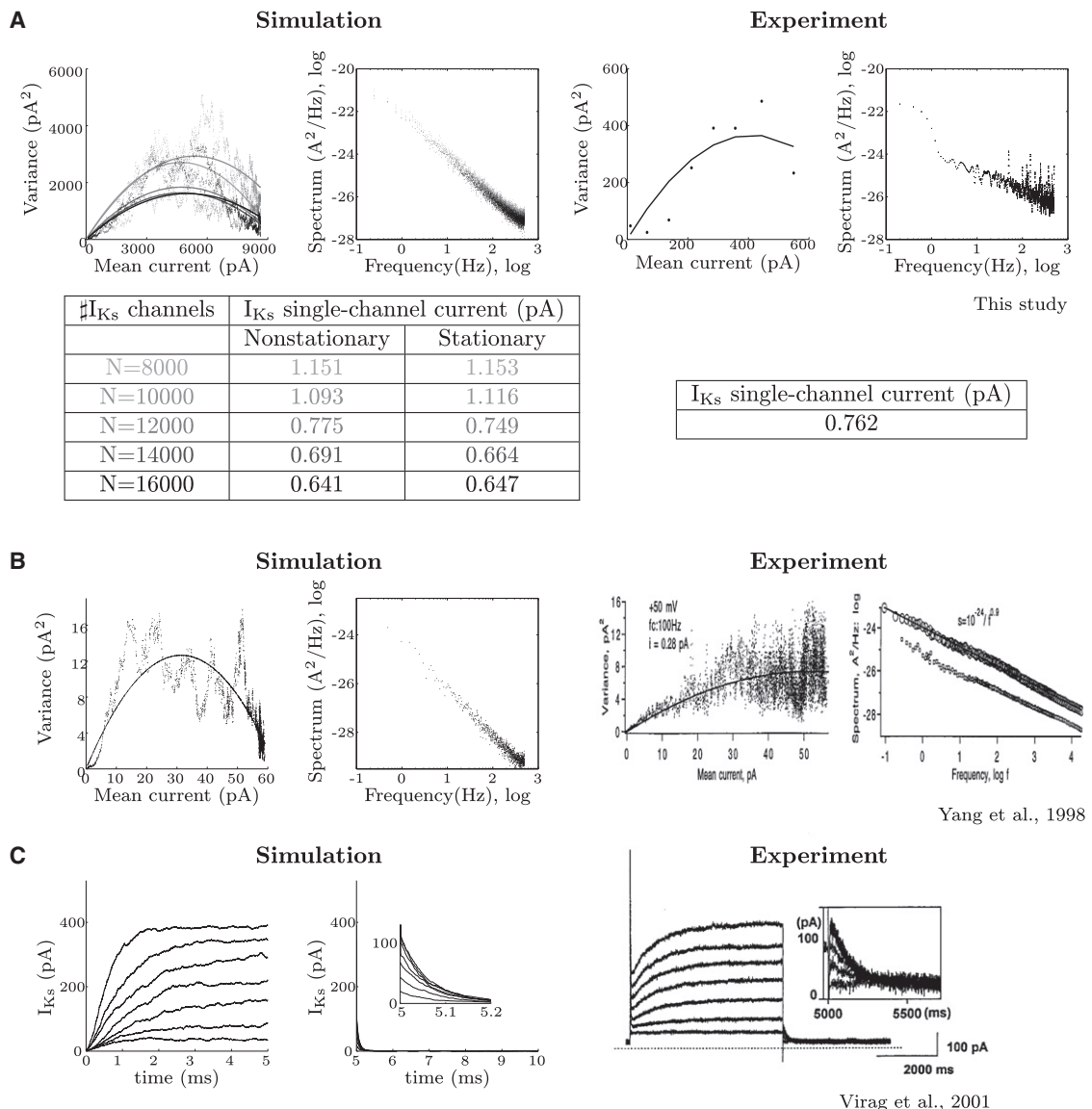


**FIGURE 1** Fluctuation analysis. (A) Nonstationary (variance-mean plots) and stationary (averaged PSDs) fluctuation analysis of simulated and experimental human  $I_{Ks}$  currents. Simulation results are computed from 20 sweeps for different numbers,  $n_{Ks}$ , of  $I_{Ks}$  channels: 8000, 10,000, 12,000, 14,000, and 16,000. Single channel current estimates are shown in each case. (B) Simulated and experimental (28) mean-variance plots and PSDs of human  $I_{Ks}$  currents at 50 mV. (C) Human  $I_{Ks}$  current traces, in simulations and experiments (24), following 5000-ms depolarizing voltage pulses from -40 mV to test potentials ranging from -10 to 50 mV in 10 mV-increments. In the simulations shown in B and C,  $n_{Ks}$  and the maximum  $I_{Ks}$  conductance,  $G_{Ks}$ , have been scaled down to match the maximum  $I_{Ks}$  amplitude of the experimental studies.

characteristics of simulated human  $I_{Ks}$  current fluctuations, Fig. 1 A presents variance-mean plots of  $I_{Ks}$  traces at 50 mV (top first panel), their averaged PSDs (top second panel), and estimated single channel currents (bottom left panel), for different channel numbers while keeping constant the maximum epicardial  $I_{Ks}$  conductance ( $G_{Ks}$ ). That is, in all the simulations of Fig. 1 A  $G_{Ks}$  ( $= n_{Ks} i_{Ks}$ ) was kept at the constant value defined in the deterministic TP06 model, while in each case  $n_{Ks}$  was given a certain value (ranging from 8000 to 16,000) and  $i_{Ks}$  was correspondingly estimated from the fluctuation analysis applied to the simulated  $I_{Ks}$  traces).

Also shown in Fig. 1 is a comparison between our stochastic simulations and previous experimental studies of the literature (24,28), both in terms of fluctuation noise analysis (Fig. 1 B) and of  $I_{Ks}$  current traces (Fig. 1 C). Because  $I_{Ks}$  amplitude is very sensitive to the experimental cell isolation procedure (32) and presents wide variations across studies (24,28),  $n_{Ks}$  and  $G_{Ks}$  in the stochastic simulations of Fig. 1, B and C, were scaled to match the maximum  $I_{Ks}$  amplitude of the corresponding experimental set of data. Specifically, we assumed that during cell isolation the unitary conductance remains unaltered but a number of  $I_{Ks}$  channels are damaged. Therefore, we reduced  $n_{Ks}$  and  $G_{Ks}$

by the same percentage in each case so that the maximum  $I_{Ks}$  amplitude in the simulations equaled the maximum  $I_{Ks}$  amplitude of the experimental set.

According to the results shown in **Fig. 1**, the time and frequency patterns of the simulated  $I_{Ks}$  currents are in good agreement with the experimental ones, indicating that our stochastic  $I_{Ks}$  model is able to reproduce intrinsic noise properties of experimental traces. Additional results on the contribution of ion channel fluctuations to macroscopic  $I_{Ks}$  variability are presented in the text and **Fig. S1** of the **Supporting Material**, concluding that a large portion of the experimental cell-to-cell differences in  $I_{Ks}$  current properties can be explained by differences in  $I_{Ks}$  channel numbers (extrinsic noise) rather than by  $I_{Ks}$  random gating (intrinsic noise). Results shown later in the study were obtained with the  $n_{Ks}$  values derived from the fluctuation analysis with no subsequent scaling, which was only applied when comparing simulated and experimental  $I_{Ks}$  current values (i.e., in **Fig. 1, B** and **C**, and **Fig. S1**).

### Channel numbers determine temporal and spatial electrophysiological heterogeneity

The impact of  $I_{Ks}$  fluctuations on temporal cell variability was investigated by using the developed and validated stochastic cell models and the previously identified channel numbers. **Fig. S2** shows examples of beat-to-beat variability in action potential duration (APD) in isolated guinea pig (**Fig. S2 A**) and human (**Fig. S2 B**) ventricular myocytes. APs were obtained for 20 consecutive cardiac cycles from simulations and experiments at 1 Hz steady-state pacing (0.5 Hz for the study by Zaniboni et al. (7)). In simulated guinea pig myocytes, averaged temporal APD ranges (computed from a set of 15 independent stochastic realizations) were 6/10/4 ms for endo/mid/epi cells. In the guinea pig experiments of this study shown in **Fig. S2 A**, APD ranges were 10, 10, 14, and 12 ms for representative apical-epi, apical-endo, basal-epi, and basal-endo cells, respectively, and in the experiment of Zaniboni et al. (7) the APD range was 25 ms. In human, simulated APD ranges were 10/15/10 ms for endo/mid/epi cells, whereas in the experiment of this study the range was 18 ms. Additionally, canine experiments were performed in this study, where the averaged range of APD temporal variability was 13 ms. A major conclusion is the confirmation that differences in  $I_{Ks}$  channel numbers determine temporal variability in the AP in the three cell layers. In both species, the lower number of  $I_{Ks}$  channels in mid cells, as compared to endo and epi cells, translated into larger beat-to-beat variability in APD, with variability being larger in human than in guinea pig—see the **Supporting Material** for further results and discussion. In all cases, AP temporal variability in the simulations was in the experimentally observed range.

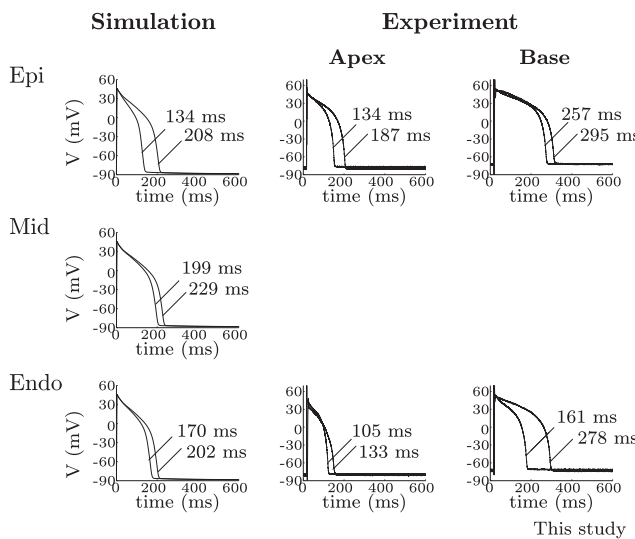
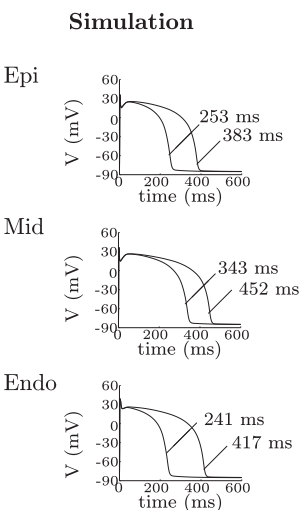
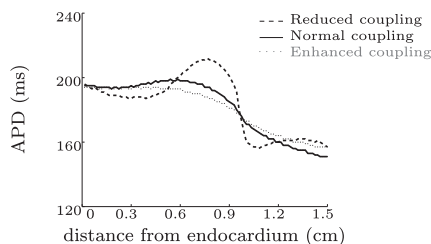
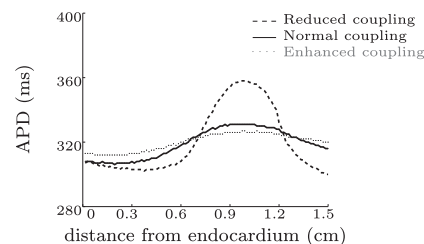
Next, cell-to-cell variability was investigated by additionally introducing extrinsic noise in the simulations, with the

number of  $I_{Ks}$  channels for each simulated cell extracted from a truncated Gaussian distribution with mean equal to the  $n_{Ks}$  value provided previously. Simulated cell-to-cell APD variability in guinea pig and human is shown in **Fig. 2**, and compared with experiments performed in isolated ventricular myocytes. In the left part of **Fig. 2 A** and in **Fig. 2 B**, simulated guinea pig and human APs associated with minimum and maximum APD values over 15 stochastic realizations, corresponding to 15 different simulated myocytes, are presented. Results are grouped according to layer in the ventricular wall, and correspond to the same simulated beat under steady-state pacing at 1 Hz. Large differences were observed in the APDs of two distinct myocytes, even when simulated from the same ventricular layer, with maximal differences of 32/30/74 ms for simulated endo/mid/epi guinea pig cells and 176/109/130 ms for human. The simulated guinea pig values were within the experimental APD differences measured in this study for myocytes isolated from the same location and heart, as shown by the representative examples in the right part of **Fig. 2 A**. Notably larger experimental differences were observed when comparing myocytes from the same location but different hearts. A summary of guinea pig and human cell-to-cell APD differences in simulations and experiments is presented in the bar charts of **Fig. S3**, with simulated differences always lying within experimental ranges (33,34).

### Cellular coupling mitigates manifestation of ion channel fluctuations in ventricles

The impact of ion channel fluctuations was evaluated when cells were coupled in a transmural 1D fiber and in an anatomically based ventricular geometry, with both intrinsic and extrinsic noises included in the  $I_{Ks}$  current formulation. The effect of coupling on temporal variability was first assessed. Simulated beat-to-beat APD variability is presented in **Fig. 3 A (left panel)**, for an electrically coupled guinea pig mid cell of the transmural fiber and an isolated mid cell. Electrotonic coupling results in a 90% reduction in the APD range over 20 consecutive cardiac cycles at 1 Hz pacing. Simulations using the whole ventricular geometry confirmed the results obtained from the 1D cable. In endo and epi guinea pig cells, percentages of reduction were 83% and 75%, respectively. In the experiments of Zaniboni et al. (7), coupling reduced the APD range by 51% (**Fig. 3 A, right panel**). In our human simulations, coupling reduced the APD range in epi, endo, and mid cells by 80%, 80%, and 87%, consistent with a 72% reduction in human experimental data (**Fig. 3 B**). In dog experiments, the averaged APD range decreased by 69%. Further results on mitigation of temporal variability due to the effect of coupling are presented in the **Supporting Material** (expressed in relative terms as coefficient of variation).

The effect of coupling on modulating spatial variability was also investigated. Cell-to-cell APD differences between

**A Guinea pig****B Human****C Guinea pig****D Human**

**FIGURE 2** Spatial APD variability. (A) Simulated and experimental APs of guinea pig myocytes at 1 Hz pacing, corresponding to minimum and maximum APD across cells ( $n = 15$  for simulations, and  $n = 2, 2, 2$  and  $4$  for experiments). (B) Analogous results in human ( $n = 15$  for simulations). (C and D): APD profiles in simulated guinea pig and human 1D fibers, computed at 1 Hz steady state for three degrees of coupling (reduced, normal, and enhanced).

the coupled myocytes of the simulated transmural fiber are shown in Fig. 2 for guinea pig (panel C) and human (panel D). APD profiles are presented for three different degrees of coupling representing reduced, normal, and enhanced electrical coupling. The diffusion coefficient for each case was 0.165 (0.234), 0.826 (1.171), and 1.487 (2.108)  $\text{cm}^2/\text{s}$  in guinea pig (human), respectively, and averaged conduction velocities at 1 Hz steady-state pacing were 14.9 (22.7), 45.5 (60.0), and 62.5 (83.3)  $\text{cm}/\text{s}$  in guinea pig (human), respectively. As illustrated in Fig. 2, coupling acted to decrease spatial APD variability across the wall and within each of the three layers. Specifically, maximal APD differences within the mid layer of the guinea pig (respectively human) 1D fiber were 28 (22), 23 (5), and 19 (3) ms under reduced, normal, and enhanced coupling, respectively, as compared with 30 (109) ms found for isolated mid myocytes. Those tissue APD differences obtained with the stochastic model in the mid layer were relatively close,  $\pm 6$  ( $\pm 2$ ) ms, to those found for the deterministic model. The maximum transmural difference in APD in the stochastic simulations was of 45 (25) ms for guinea pig (human) under normal coupling, and it increased by 27 (144)% and decreased by 11 (36)% under reduced and enhanced coupling, respec-

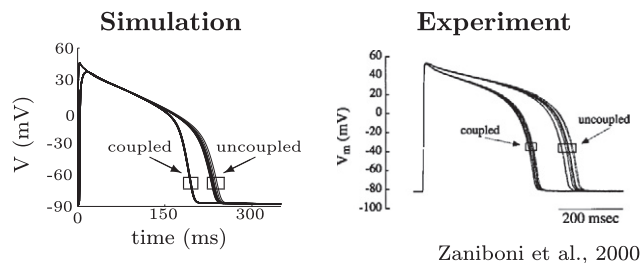
tively. In both guinea pig and human, transmural APD differences obtained with the stochastic model were only slightly different ( $\pm 2$  ms) from those found with the deterministic model. All the previous results show that, in tissue, intercellular coupling acts to suppress the important role of  $I_{\text{Ks}}$  stochasticity in modulating beat-to-beat and cell-to-cell variability in APD observed in isolated cardiomyocytes.

Finally, the manifestation of  $I_{\text{Ks}}$  stochasticity was investigated in pseudo-ECGs (see text and Fig. S4 in the Supporting Material). Temporal variability in the pseudo-ECG is shown to be of very low magnitude under control conditions, but reduced coupling acted to slightly unmask temporal fluctuations in the pseudo-ECG.

### Pathology accentuates the proarrhythmic consequences of ion channel fluctuations

In this study, we hypothesize that pathological conditions affecting repolarization reserve might potentiate the role of stochastic  $I_{\text{Ks}}$  gating in modulating variability in APD. Our simulations show that  $I_{\text{Kr}}$  block increased temporal APD variability in guinea pig and human. In both cases, the increase was more prominent in mid cells than in endo-

## A Guinea pig



## B Human

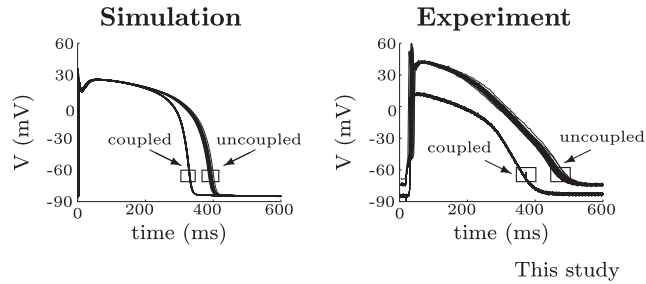


FIGURE 3 Temporal variability in uncoupled and coupled mid myocytes from simulations and experiments (measured in this study and reproduced from (7) for guinea pig (A) and human (B)).

and epi cells due to differences in channel numbers (>8000% increase in guinea pig due to abnormal depolarizations interrupting AP repolarization and 92% increase in human in mid cells, as compared to >8000% and 30%, respectively, in endo and 25% and 20%, respectively, in epi cells). Elevated temporal variability due to  $I_{Kr}$  block was also observed for cells coupled into tissue with elevated variability being also more prominent in the midmyocardial region due to its associated lower number of  $I_{Ks}$  channels (188%, 213%, and 61% increase in APD range for cells in the central part of endo, mid, and epi regions within the simulated guinea pig 1D fiber, and 8%, 27%, and 23% for the human 1D fiber). Our results are consistent with observations from experimental studies reported in the literature (7,35,36) and with the experiment on a human myocyte conducted in this study, where the APD range was increased by 278% after blocking  $I_{Kr}$ . In addition, the canine experiments of this study confirmed our observation that the increase in the APD range after dofetilide injection (full  $I_{Kr}$  block) was more prominent in single cells than in tissue, with averaged increases of 370% and 39%, respectively.

$I_{Kr}$  block also accentuated cell-to-cell APD differences in isolated myocytes and spatial APD dispersion in tissue. In the 1D tissue simulations, transmural APD differences at normal coupling were of 174 and 34 ms under full  $I_{Kr}$  block in guinea pig and human, respectively, which represent around 4 and 1.5 times the APD variability values found in control.

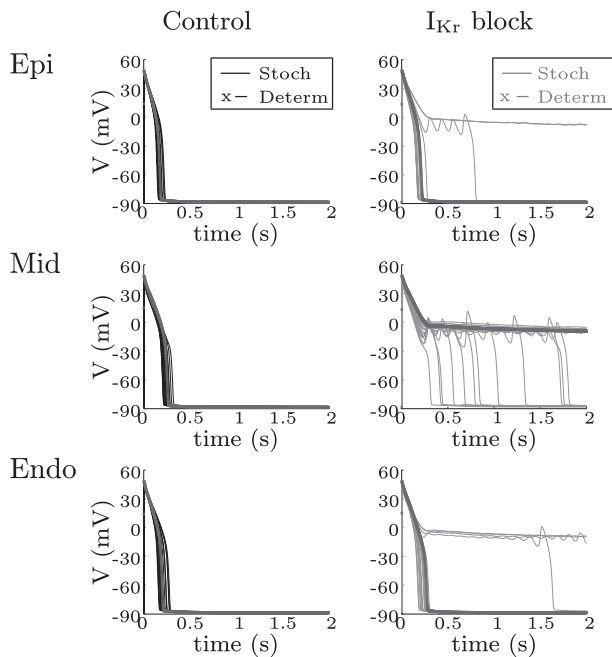
Under  $I_{Kr}$  block, there were increases in the temporal ranges of the QT interval of 526% in guinea pig and 43%

in human (see the Supporting Material). Nevertheless, the variability levels observed after blocking  $I_{Kr}$  were only of some relevance when measured in single cells, but not in tissue or ECG at physiological coupling due to the effect of electrotonic interactions working to synchronize APDs of neighboring cells (7). Simulation of reduced coupling conditions, as documented in diseased hearts, confirmed the role of temporal repolarization variability in facilitating the occurrence of electrical instabilities, as seen by complex patterns of APD and QT Poincaré plots, in accord with experimental and clinical data (1,2,37) (see Fig. S4 and text in the Supporting Material).

Of importance, our simulations show that  $I_{Ks}$  stochastic fluctuations in the presence of  $I_{Kr}$  block favored the appearance of repolarization abnormalities such as early afterdepolarization (EAD) formation (2,3). EAD occurrence was promoted by a sudden change in the stimulation frequency from 1 to 0.4 Hz (Fig. 4). In guinea pig cells,  $I_{Kr}$  blockade in the deterministic model only resulted in EADs in mid cells, while with stochastic  $I_{Ks}$ , EADs occurred in 21/95/16% of endo/mid/epi cells. In human, EADs was not observed in the deterministic model for any cell type under  $I_{Kr}$  block. However, the consideration of  $I_{Ks}$  fluctuations in the model led to EADs in 20% of the simulations for mid cells. The ability of  $I_{Kr}$  block to produce EADs, more so in mid cells than in endo or epi cells, reported from the stochastic simulations of this study is in agreement with findings from experiments conducted in different species, including guinea pig and human (35,38–40) and also with the canine experiments of this study, where EADs developed in 50% (2 out of 4) of the analyzed cells after dofetilide injection—Fig. 5 A.

Coupling acted to modulate the likelihood of EAD occurrence in tissue following rate deceleration. In the presence of  $I_{Ks}$  stochasticity, EADs were observed after full  $I_{Kr}$  block in one-fifth of the guinea pig 1D tissue containing endo and mid cells, but were not observed when simulating the whole ventricular geometry. When coupling was moderately decreased by 30%, the 1D tissue portion presenting EADs was enlarged, occupying one-third of the tissue (endo-mid region). In human tissue, EADs was not seen in any simulation, consistent with the results of the canine experiments of this study, where EADs was not induced in tissue exposed to dofetilide (Fig. 5 B). Furthermore, nor even after simulating 80% coupling reduction could EADs be observed in human tissues. Our results show that  $I_{Ks}$  stochasticity enhances the probability of EAD formation, whereas electrotonic flow due to intercellular coupling counteracts this effect. This could have major implications for the genesis of arrhythmias as it suggests that under normal coupling it is difficult for those EADs to develop and propagate, even if  $I_{Kr}$  is fully blocked. However, abnormal conditions involving reduced levels of cell-to-cell coupling, as in heart failure or myocardial ischemia, could render the myocardium more vulnerable to the occurrence of EADs following  $I_{Kr}$  block,

## A Guinea pig



## B Human

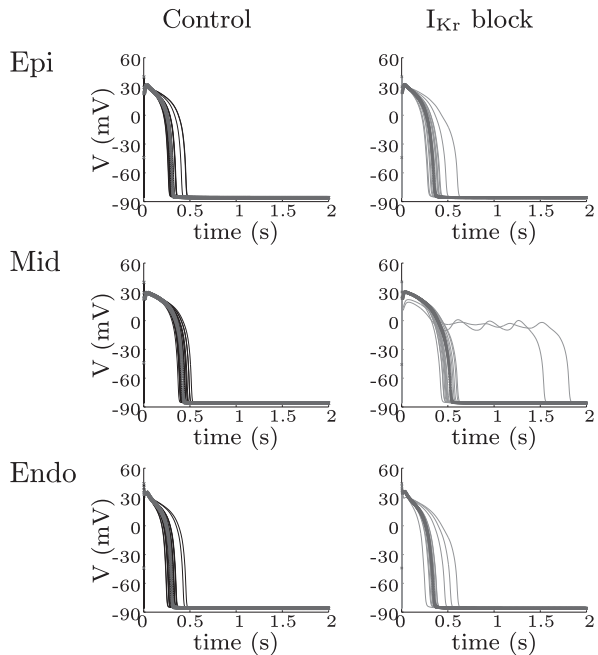


FIGURE 4 | EAD generation. (A) Simulated APs obtained after suddenly changing pacing rate from 1 to 0.4 Hz using the deterministic FR07 guinea pig model (black dashed for control, and gray dashed for  $I_{Kr}$  block) and 20 different realizations of the stochastic guinea pig model (black solid for control, and gray solid for  $I_{Kr}$  block). (B) Analogous results for human.

which could in turn trigger arrhythmias if they occurred in a substantial mass of the ventricle.

Increased temporal variability due to  $I_{Ks}$  fluctuations also facilitates the occurrence of APD alternans. APD alternans,

defined as alternations in the APD of the form long-short-long-short, occur at rapid rates of stimulation and have been shown to be predictive of arrhythmia development (5). In this study, the threshold frequency for APD alternans was determined as the lowest frequency for which differences in APD values of at least eight consecutive beats were  $>10$  ms (41). That threshold was found to be lowered when stochastic  $I_{Ks}$  fluctuations were introduced into the deterministic models; particularly under  $I_{Kr}$  block conditions (see text and Fig. S5 in the Supporting Material).

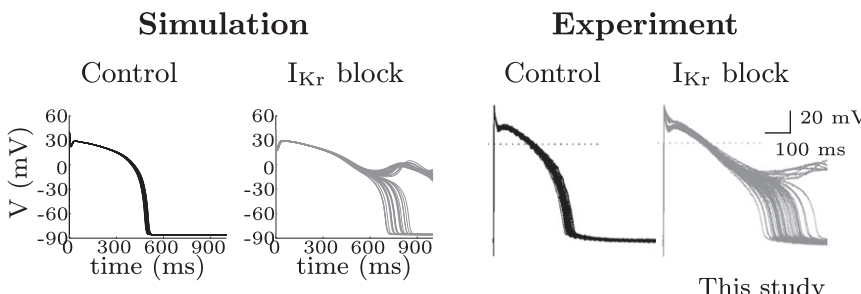
Repolarization alternans were not observed in physiologically coupled tissue (transmural 1D fiber or whole ventricular geometry) at any stimulation frequency either under control or full  $I_{Kr}$  block, but were observed in the mid layer at reduced coupling. The thresholds for APD alternans in tissue were of 8.3 and 3.3 Hz in guinea pig and human under control, and 5.7 and 2.9 Hz under  $I_{Kr}$  block, in both cases after 80% coupling reduction. These results on the increased likelihood of APD alternans (as an extreme form of beat-to-beat variability) in diseased hearts presenting reduced levels of electrotonic coupling are in agreement with experimental data (42).

## Study limitations and future research

This combined experimental and theoretical study provides an in-depth characterization of the role played by intrinsic and extrinsic noise due to  $I_{Ks}$  channel gating and cell-to-cell differences in  $I_{Ks}$  density in determining variability in cardiac repolarization. The following points include a number of questions arising from the current study that remain to be addressed through further research:

1. Cell and tissue AP models were developed where the  $I_{Ks}$  current was modeled as a stochastic process but all of the other model components were deterministic. The  $I_{Ks}$  characteristics of slow kinetics and small associated number of channels suggest an important contribution to repolarization variability (9). However, modeling intrinsic and extrinsic noises in other transmembrane ionic currents and calcium dynamics would allow identifying the most relevant causes of APD variability. This was attempted in recent computational studies (see, for instance (13,16)), and experimental confirmation is required.
2. Attention was focused on variability that originates under constant pacing rates and autonomic influences were not at all considered. Future studies should investigate the effects of  $I_{Ks}$  stochasticity on cell and tissue variability in situations involving high levels of  $\beta$ -adrenergic stimulation, where the role of  $I_{Ks}$  has been suggested to be more relevant (8).
3. Other electrophysiological sources not modeled in this study may additionally contribute to repolarization variability, including differences in cell geometry or

## A Single cell



## B Tissue

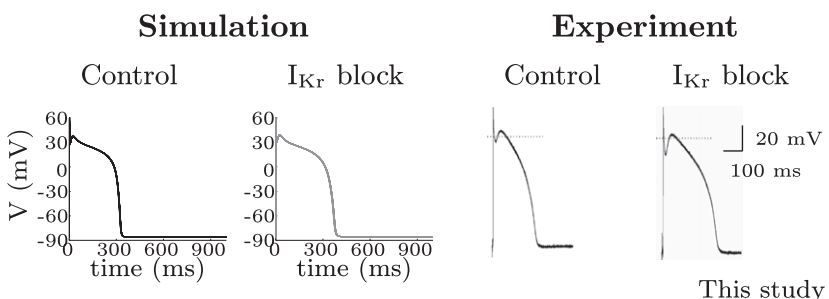


FIGURE 5 Temporal variability and presence/absence of EADs in single cell (A) and tissue (B) from human simulations and canine experiments under control (black line) and following  $I_{Kr}$  block (gray line).

tissue structure, and heterogeneities in electrotonic coupling (37).

4. The  $I_{Ks}$  current in the deterministic TP06 human ventricular model, taken as the basis for our stochastic human model, is much larger than in experimental studies (24,28) and other human ventricular cell models recently published (43,44). Because  $I_{Ks}$  density is large in the model, there are an associated high number of  $I_{Ks}$  channels, and, as a consequence, the effects of channel gating on cell and tissue variability are attenuated. The results of our study in human myocytes could be interpreted as providing a lower limit for the effects of  $I_{Ks}$  stochasticity on repolarization variability and associated arrhythmogenic implications.
5. The bandwidth of the experimental recordings has a notable influence in the fluctuation analysis. If the bandwidth is not sufficient, the variance of the current fluctuations is underestimated, which correspondingly leads to underestimates of unitary current. This in turn implies a larger number of  $I_{Ks}$  channels in the model, and reduced variability at all levels. Experimental studies using data sampled at frequencies varying from 0.25 to 25 kHz have shown that below 10 kHz the conductance values obtained from fluctuation analysis are affected by a lack of convergence of the current variance. In this study, experimental  $I_{Ks}$  current traces recorded in human myocytes were filtered at 1 kHz. Based on this, we acknowledge a limitation for a more accurate evaluation of  $I_{Ks}$  channel noise. An illustration of the potential effects that larger  $I_{Ks}$  noise levels, accounting for higher frequency components in experimental  $I_{Ks}$  traces, may

have on APD variability and arrhythmogenesis is presented in Fig. S6, showing results obtained by decreasing  $n_{Ks}$  while keeping  $G_{Ks}$  constant. Despite the acknowledged limitation, the unitary current of  $I_{Ks}$  channels estimated in this study was 0.762 pA, which is very similar to the  $0.6 \pm 0.2$  pA found by Yang et al. (28), and  $0.8 \pm 0.2$  pA found by Sesti et al. (30) for human  $I_{Ks}$  currents expressed in *Xenopus* oocytes, which were exclusively used in this study for comparison purposes. In terms of  $I_{Ks}$  unitary conductance, the estimated value from our experiments was 5.8 pS, which is comparable to the 6.6 pS found in (30) for a corresponding cut-off frequency of 1 kHz. Future studies should evaluate the impact of the filter cut-off frequency on the estimation of single channel current/unitary conductance of membrane ionic currents from intact human myocytes.

## CONCLUSIONS

In this study, a combined experimental and computational multiscale investigation is conducted to unravel the role played by  $I_{Ks}$  stochasticity in modulating beat-to-beat and cell-to-cell variability in ventricular repolarization. To the best of our knowledge, this is the first study where careful construction and validation of mathematical models of  $I_{Ks}$  stochasticity is performed to guarantee reliable conclusions on its role in determining ventricular repolarization variability in health and disease. The results suggest that stochastic  $I_{Ks}$  gating and channel numbers are important contributors to temporal and spatial variability in isolated

cells, but their effects are masked in tissue due to electrotonic interactions. Pathological conditions resulting in reduced repolarization reserve (e.g.,  $I_{Kr}$  block) or in intercellular uncoupling (e.g., acidosis) could uncover the manifestation of stochastic  $I_{Ks}$  properties resulting in enhanced variability and proarrhythmic abnormalities in repolarization such as afterdepolarizations and alternans.

## SUPPORTING MATERIAL

Further details and results, references, and six figures are available at [http://www.biophysj.org/biophysj/supplemental/S0006-3495\(11\)01241-0](http://www.biophysj.org/biophysj/supplemental/S0006-3495(11)01241-0).

The authors are grateful to Christian Bollendorff and Peter Kohl for their contribution to the guinea pig experiments. The authors thank the reviewers for their valuable comments.

This study was supported by the European Commission preDiCT grant (DG-INFSO-224381), UK Medical Research Council Career Development Award (B.R.), Royal Society International Joint Project (E.P., B.R.), grant TEC2010-19410 from Ministerio de Ciencia e Innovación, PI 144/2009 and T30 from Gobierno de Aragón, Spain (E.P.), and grants OTKA CNK-77855 from Hungarian Scientific Research Fund, TECH\_08\_A1\_CARDIO08 from National Office Research and Technology–Ányos Jedlik Programme, and TÁMOP-4.2.2-08/1-2008-0013 and TÁMOP-4.2.1/B-09/1/KONV-2010-0005 National Development Agency cofinanced by the European Regional Fund, Hungary (L.V., N.J., T.S., A.V., N.S., P.P.N.).

## REFERENCES

1. Hondeghem, L. M., L. Carlsson, and G. Duker. 2001. Instability and triangulation of the action potential predict serious proarrhythmia, but action potential duration prolongation is antiarrhythmic. *Circulation*. 103:2004–2013.
2. Thomsen, M. B., S. C. Verduyn, ..., M. A. Vos. 2004. Increased short-term variability of repolarization predicts d-sotalol-induced torsades de pointes in dogs. *Circulation*. 110:2453–2459.
3. Johnson, D. M., J. Heijman, ..., P. G. Volders. 2010.  $I_{(Ks)}$  restricts excessive beat-to-beat variability of repolarization during beta-adrenergic receptor stimulation. *J. Mol. Cell. Cardiol.* 48:122–130.
4. Hinterseer, M., B. M. Beckmann, ..., S. Käab. 2010. Usefulness of short-term variability of QT intervals as a predictor for electrical remodeling and proarrhythmia in patients with nonischemic heart failure. *Am. J. Cardiol.* 106:216–220.
5. Myles, R. C., F. L. Burton, ..., G. L. Smith. 2008. The link between repolarization alternans and ventricular arrhythmia: does the cellular phenomenon extend to the clinical problem? *J. Mol. Cell. Cardiol.* 45:1–10.
6. Lerma, C., T. Krogh-Madsen, ..., L. Glass. 2007. Stochastic aspects of cardiac arrhythmias. *J. Stat. Phys.* 128:347–374.
7. Zaniboni, M., A. E. Pollard, ..., K. W. Spitzer. 2000. Beat-to-beat repolarization variability in ventricular myocytes and its suppression by electrical coupling. *Am. J. Physiol. Heart Circ. Physiol.* 278:H677–H687.
8. Severi, S., C. Corsi, ..., A. Zaza. 2009. Mechanisms of beta-adrenergic modulation of  $I_{(Ks)}$  in the guinea-pig ventricle: insights from experimental and model-based analysis. *Biophys. J.* 96:3862–3872.
9. Krogh-Madsen, T. 2004. Effects of single-channel noise on spontaneous beating and the phase-resetting response of cardiac oscillators. PhD thesis. McGill University, Montreal, Canada.
10. Fox, R. F. 1997. Stochastic versions of the Hodgkin-Huxley equations. *Biophys. J.* 72:2068–2074.
11. Mino, H. J., J. T. Rubinstein, and J. A. White. 2002. Comparison of algorithms for the simulation of action potentials with stochastic sodium channels. *Ann. Biomed. Eng.* 30:578–587.
12. Ponard, J. G., A. A. Kondratyev, and J. P. Kucera. 2007. Mechanisms of intrinsic beating variability in cardiac cell cultures and model pacemaker networks. *Biophys. J.* 92:3734–3752.
13. Tanskanen, A. J., J. L. Greenstein, ..., R. L. Winslow. 2005. The role of stochastic and modal gating of cardiac L-type  $Ca^{2+}$  channels on early after-depolarizations. *Biophys. J.* 88:85–95.
14. Sato, D., L. H. Xie, ..., Z. Qu. 2009. Synchronization of chaotic early afterdepolarizations in the genesis of cardiac arrhythmias. *Proc. Natl. Acad. Sci. USA.* 106:2983–2988.
15. Silva, J. R., H. Pan, ..., Y. Rudy. 2009. A multiscale model linking ion-channel molecular dynamics and electrostatics to the cardiac action potential. *Proc. Natl. Acad. Sci. USA.* 106:11102–11106.
16. Lemay, M., E. de Lange, and J. P. Kucera. 2011. Effects of stochastic channel gating and distribution on the cardiac action potential. *J. Theor. Biol.* 281:84–96.
17. Pueyo, E., A. Corrias, D. Gavaghan, K. Burrage, and B. Rodríguez. 2009. Role of  $I_{Ks}$  gating kinetics in arrhythmogenesis. *Heart Rhythm, Supplement, Abstract*, S296.
18. ten Tusscher, K. H., and A. V. Panfilov. 2006. Alternans and spiral breakup in a human ventricular tissue model. *Am. J. Physiol. Heart Circ. Physiol.* 291:H1088–H1100.
19. Faber, G. M., J. Silva, ..., Y. Rudy. 2007. Kinetic properties of the cardiac L-type  $Ca^{2+}$  channel and its role in myocyte electrophysiology: a theoretical investigation. *Biophys. J.* 92:1522–1543.
20. Van Kampen, N. G. 1992. Stochastic Processes in Physics and Chemistry. North-Holland, Amsterdam.
21. Gima, K., and Y. Rudy. 2002. Ionic current basis of electrocardiographic waveforms: a model study. *Circ. Res.* 90:889–896.
22. Corrias, A., X. Jie, ..., B. Rodriguez. 2010. Arrhythmic risk biomarkers for the assessment of drug cardiotoxicity: from experiments to computer simulations. *Philos. Transact. A Math. Phys. Eng. Sci.* 368: 3001–3025.
23. Hille, B. 2001. Ion Channels of Excitable Membranes. Sinauer Associates, Sunderland, MA.
24. Virág, L., N. Iost, ..., J. G. Papp. 2001. The slow component of the delayed rectifier potassium current in undiseased human ventricular myocytes. *Cardiovasc. Res.* 49:790–797.
25. Sigworth, F. J. 1980. The variance of sodium current fluctuations at the node of Ranvier. *J. Physiol.* 307:97–129.
26. Lingle, C. J. 2006. Empirical considerations regarding the use of ensemble-variance analysis of macroscopic currents. *J. Neurosci. Methods.* 158:121–132.
27. Sigworth, F. J. 1981. Interpreting power spectra from nonstationary membrane current fluctuations. *Biophys. J.* 35:289–300.
28. Yang, Y., and F. J. Sigworth. 1998. Single-channel properties of  $I_{Ks}$  potassium channels. *J. Gen. Physiol.* 112:665–678.
29. Walsh, K. B., J. P. Arena, ..., R. S. Kass. 1991. Delayed-rectifier potassium channel activity in isolated membrane patches of guinea pig ventricular myocytes. *Am. J. Physiol.* 260:H1390–H1393.
30. Sesti, F., and S. A. Goldstein. 1998. Single-channel characteristics of wild-type  $I_{Ks}$  channels and channels formed with two minK mutants that cause long QT syndrome. *J. Gen. Physiol.* 112:651–663.
31. Furukawa, T., S. Kimura, ..., R. J. Myerburg. 1992. Potassium rectifier currents differ in myocytes of endocardial and epicardial origin. *Circ. Res.* 70:91–103.
32. Yue, L., J. Feng, ..., S. Nattel. 1996. Transient outward and delayed rectifier currents in canine atrium: properties and role of isolation methods. *Am. J. Physiol.* 270:H2157–H2168.
33. Bryant, S. M., X. Wan, ..., G. Hart. 1998. Regional differences in the delayed rectifier current ( $I_{Kr}$  and  $I_{Ks}$ ) contribute to the differences in action potential duration in basal left ventricular myocytes in guinea-pig. *Cardiovasc. Res.* 40:322–331.

34. Li, G. R., J. Feng, ..., M. Carrier. 1998. Transmural heterogeneity of action potentials and Ito1 in myocytes isolated from the human right ventricle. *Am. J. Physiol.* 275:H369–H377.

35. Sicouri, S., M. Quist, and C. Antzelevitch. 1996. Evidence for the presence of M cells in the guinea pig ventricle. *J. Cardiovasc. Electrophysiol.* 7:503–511.

36. Bargheer, K., F. Bode, ..., P. R. Lichtlen. 1994. Prolongation of monophasic action potential duration and the refractory period in the human heart by tedisamil, a new potassium-blocking agent. *Eur. Heart J.* 15:1409–1414.

37. Poelzing, S., and D. S. Rosenbaum. 2004. Nature, significance, and mechanisms of electrical heterogeneities in ventricle. *Anat. Rec. A Discov. Mol. Cell. Evol. Biol.* 280:1010–1017.

38. Spitzer, K. W., A. E. Pollard, ..., D. J. Huelsing. 2006. Cell-to-cell electrical interactions during early and late repolarization. *J. Cardiovasc. Electrophysiol.* 17 (Suppl 1):S8–S14.

39. Veldkamp, M. W., A. O. Verkerk, ..., T. Ophof. 2001. Norepinephrine induces action potential prolongation and early afterdepolarizations in ventricular myocytes isolated from human end-stage failing hearts. *Eur. Heart J.* 22:955–963.

40. Burashnikov, A., and C. Antzelevitch. 2002. Prominent I(Ks) in epicardium and endocardium contributes to development of transmural dispersion of repolarization but protects against development of early afterdepolarizations. *J. Cardiovasc. Electrophysiol.* 13:172–177.

41. Wan, X., K. R. Laurita, ..., D. S. Rosenbaum. 2005. Molecular correlates of repolarization alternans in cardiac myocytes. *J. Mol. Cell. Cardiol.* 39:419–428.

42. Kjølbye, A. L., M. Dikshteyn, ..., D. S. Rosenbaum. 2008. Maintenance of intercellular coupling by the antiarrhythmic peptide rotigapptide suppresses arrhythmogenic discordant alternans. *Am. J. Physiol. Heart Circ. Physiol.* 294:H41–H49.

43. Grandi, E., F. S. Pasqualini, and D. M. Bers. 2010. A novel computational model of the human ventricular action potential and Ca transient. *J. Mol. Cell. Cardiol.* 48:112–121.

44. O'Hara, T., L. Virág, ..., Y. Rudy. 2011. Simulation of the undiseased human cardiac ventricular action potential: model formulation and experimental validation. *PLOS Comput. Biol.* 7:e1002061.